Swiss J Geosci (2012) 105:343–360
DOI 10.1007/s00015-012-0104-6

Three generations of monazite in Austroalpine basement rocks to the south of the Tauern Window: evidence for Variscan, Permian and Eo-Alpine metamorphic events

Erwin Krenn · Bernhard Schulz · Fritz Finger

Received: 19 December 2011 / Accepted: 18 June 2012 / Published online: 3 August 2012

Abstract Three monazite generations were observed in garnet-bearing micaschists from the Schobergruppe in the basement to the south of the Tauern Window, Eastern Alps. Low-Y monazite of Variscan age (321 ± 14 Ma) and high-Y monazite of Permian age (261 ± 18 Ma) are abundant in the mica-rich rock matrix and in the outer domains of large garnet crystals. Pre-Alpine monazite commonly occurs as polyphase grains with low-Y Variscan cores and high-Y Permian rims. Monazite of Eo-Alpine age (112 ± 22 Ma) is rarer and was observed as small, partly Y-enriched grains (3 wt. % Y_2O_3) in the rock matrix and within garnet. Based on monazite-xenotime thermometry, Y + HREE values in monazite indicate minimum crystallization conditions of 500 °C during the Variscan and 650 °C for the Permian and Alpine events, respectively. Garnet zoning and thermobarometric calculations with THERMOCALC 3.21 record an amphibolite facies, high-pressure stage of ~600 °C/13–16 kbar, followed by a thermal maximum at 650–700 °C and 6–9 kbar. The Eo-Alpine age for these two events is supported by inclusions of Cretaceous monazite in the garnet domains used for thermobarometric constraints and through the high growth temperatures of Eo-Alpine monazite, which is consistent with that of the thermal maximum (~700 °C). The age and growth conditions of a few Mn-rich garnet cores, sporadically present within Eo-Alpine garnet, are unclear because inclusions of monazite, plagioclase and biotite necessary for thermobarometric- and age constraints are absent. However, based on monazite thermometry, Permian and Variscan metamorphic conditions were high enough for the growth of pre-Alpine garnet. The formation of Variscan garnet and its later resorption, plus Y-release, would also explain the high Y in Permian monazite, which cannot originate from preexisting Variscan monazite only. Monazite of Variscan, Permian and/or Eo-Alpine ages were also observed in other garnet-bearing micaschists from the Schobergruppe. This suggests that the basement of the Schobergruppe was overprinted by three discrete metamorphic events at conditions of at least lower amphibolite facies. While the Variscan event affected all parts of this basement, the younger events are more pronounced in its structurally lower units.

Keywords Austroalpine basement · Eastern Alps · Monazite · Garnet · Dating · Geothermobarometry

Editorial handling: François Bussy

E. Krenn (✉) · F. Finger
Department of Materials Engineering and Physics, University of Salzburg, 5020 Salzburg, Austria
e-mail: erwin.krenn@sbg.ac.at

B. Schulz
Institut für Mineralogie der TU Bergakademie, Brennhausgasse 14, 09596 Freiberg, Germany

1 Introduction

The Austroalpine basement immediate to the south of the Tauern Window within the Northern-Defereggen-Petzeck Group (the Schobergruppe as a part of it) was overprinted during the Eo-Alpine orogeny at variable metamorphic conditions (e.g., Schuster et al. 2004; Schmid et al. 2004; Schulz et al. 2005). According to some authors (Hoinkes et al. 1999; Linner et al. 2000) and as outlined in the metamorphic map of the Alps (Frey 1999a, b; Neubauer et al. 1999; Hoinkes et al. 1999; Schmid et al. 2004), even Eo-Alpine high-pressure amphibolite facies conditions were reached.

However it is difficult to assess the pre-Alpine metamorphic evolution in this part of the basement, in particular

the Permian and Variscan events, since the older metamorphic assemblages are mostly overprinted and common geochronometers largely re-equilibrated. Accessory phases like monazite or zircon are usually refractory even at high-grade metamorphic overprints (e.g. Rubatto et al. 2006) and may therefore better record earlier thermal events than common minerals. However, although highly refractory, monazite shows certain reactivity as well and can crystallize at almost every *P–T* conditions, including very low grades (Read et al. 1987; Evans et al. 2002; Rasmussen et al. 2001; Rasmussen and Muhling 2007, 2009; Wan et al. 2007; Wilby et al. 2007; Biševac et al. 2011). As a consequence, several generations of monazite may be observed within a single sample or even a single grain (e.g., DeWolf et al. 1993; Cocherie et al. 1998; Pyle 2006; Spear et al. 2008; Petrík and Konečný 2009; Martins et al. 2009; Schulz and von Raumer 2011).

Apart from geochronological aspects, the chemical composition of monazite is a valuable petrogenetic indicator. The incorporation of Y and HREE in monazite follows a solvus and can be used as a thermometer, the so called monazite–xenotime miscibility gap thermometer (Gratz and Heinrich 1997; Heinrich et al. 1997; Pyle et al. 2001). In addition, Y-zoning in monazite may be correlated with distinct stages of garnet growth or breakdown (Pyle and Spear 2003), as garnet highly fractionates this element. Y will thus be less available for monazite when garnet is crystallizing simultaneously and the other way around when garnet breaks down (e.g. Zhu and O'Nions 1999a, b; Pyle et al. 2001; Krenn et al. 2009; Martins et al. 2009). Therefore the Y distribution in monazite can be useful in clarifying if garnet growth occurred prior to, at the same time as or after monazite.

In this study, we present data from polymetamorphic Schobergruppe rocks hosting distinct generations of monazite with specific Y contents. Three monazite generations have been identified and corroborated by comparison with other samples from this region. Variable Y contents evidence the existence of pre-Alpine metamorphic assemblages with simultaneous crystallization of garnet (e.g., Gaidies et al. 2008; Pyle and Spear 2003).

2 Geological setting

The studied samples are micaschists from the Austroalpine basement of the Schobergruppe (provinces Carinthia and Tyrol in Austria; Fig. 1a), which in turn belongs to the Northern-Defereggen-Petzeck Group (Fig. 1b). This part of the Austroalpine basement nappe is located to the south of the central to eastern Tauern Window (Schulz 1993a, b). The samples were taken close to eclogitic amphibolites (Fig. 1b, d) described by Schulz (1993a) and Schulz et al. (2005). Other micaschist samples from the Schobergruppe or from adjacent parts of the Austroalpine basement (Fig. 1b, e) have been considered for age control. Some of them were located in areas free of Alpine overprint, according to available Carboniferous K–Ar and Rb–Sr mica ages (Fig. 1c).

As in many crystalline complexes in the Eastern Alps, the Northern-Defereggen-Petzeck Group was overprinted by Alpine metamorphism during Cretaceous times (e.g. Schuster et al. 2004; Schulz et al. 2008). This metamorphic overprint reached greenschist to high-pressure amphibolite facies conditions (Exner 1962; Oxburgh et al. 1966; Troll and Hölzl 1974; Troll et al. 1976, 1980; Schulz 1993a; Linner et al. 2000). In high-grade zones, relicts of the pre-existing Devonian-Carboniferous Variscan metamorphism are often blurred.

So far, Variscan amphibolite facies metamorphism has been reported mainly from the basement south and southeast to the Schobergruppe (Schulz 1990, 1993b; Schuster et al. 2001; Schulz et al. 2005, 2008; Steidl et al. 2009, 2010a, b), where mica cooling ages do not record significant Alpine overprint (Fig. 1c). From a tectonic point of view, the area to the south of the so-called Defereggen-Antholz-Vals shear zone (DAV) belongs to an upper part of the Austroalpine basement, while the Schobergruppe represents a structurally lower part.

Variscan ages in metapelitic basement rocks south to the Tauern Window are generally rare. Schulz et al. (2005, 2008) for instance report Variscan monazite from the Schobergruppe and Steidl et al. (2010a, b) Variscan monazite from the Michlbach Complex, in the eastern Defereggen Alps, south to the DAV. Geochronological data to the east of the Schobergruppe range from 90 to 310 Ma (Hoke 1990; Schuster et al. 2001) and are interpreted as a mixture of Variscan and Eo-Alpine ages. Similarly, Permian ages in metapelitic rocks were also interpreted as mixed ages (Carboniferous to Cretaceous) or were ascribed to a slow Variscan cooling history (e.g. Borsi et al. 1978). So far, traces of a Permian event in the Schobergruppe seem to be restricted to the emplacement of pegmatite bodies and related *HT/LP* overprint nearby. Although Permian pegmatites are very common in the basement of the Schobergruppe (Bücksteeg 1999), it is not clear if this area was also affected by a Permian *HT/LP* event as is the case in other crystalline complexes south and southeast to the Schobergruppe (Schuster and Stüwe 2008).

3 Samples

Monazite and garnet were studied in detail in three garnet-bearing micaschist samples (520, 527 and Alk 8a) located

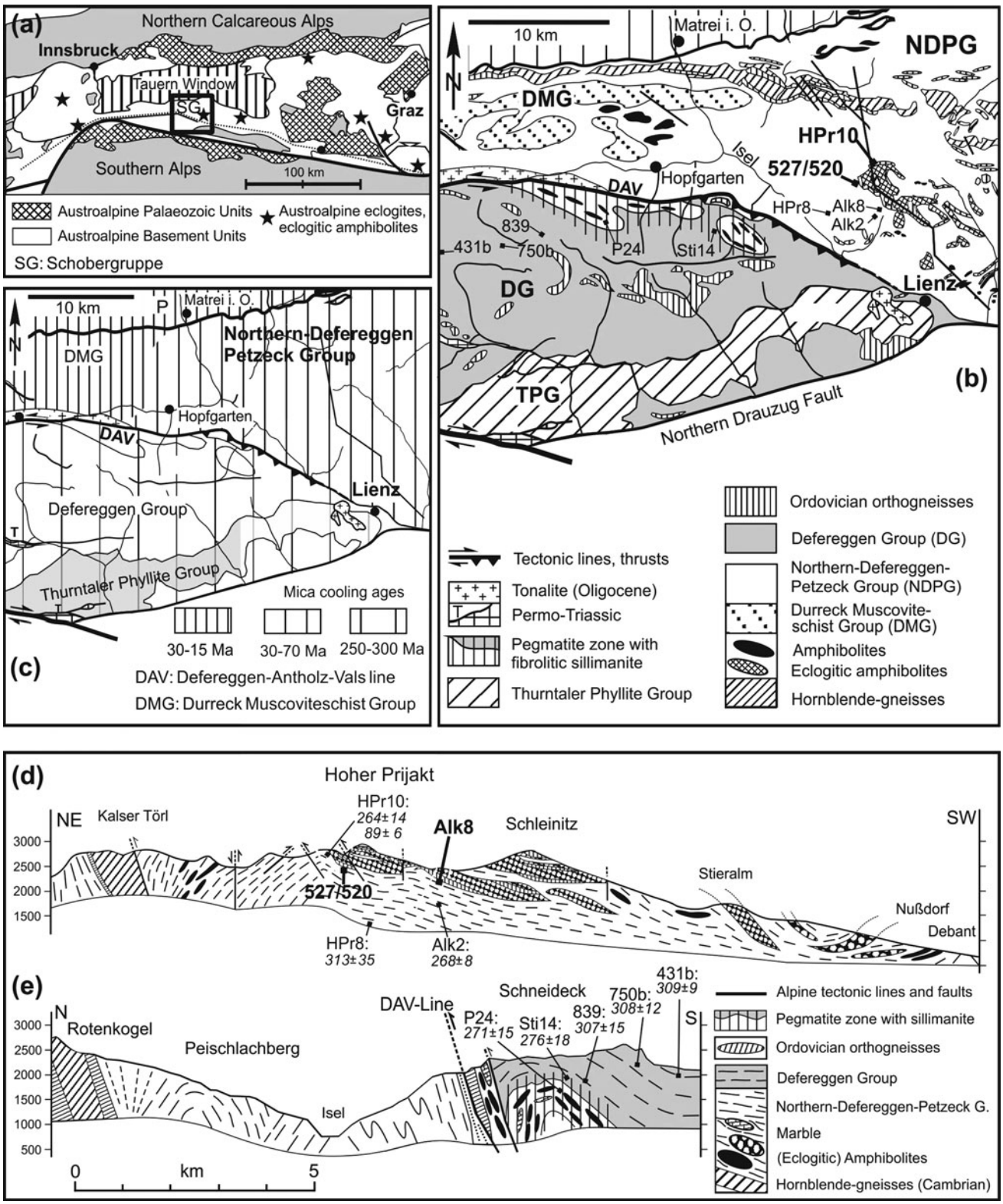

Fig. 1 Geological map showing the Schobergruppe (SG) within the tectonic framework of the Eastern Alps **(a)** and in more detail with sample location **(b)** (modified after Schulz et al. (2005, 2008). **(c)** Distribution of K–Ar and Rb–Sr mica ages to the south of the Tauern Window (compiled from Borsi et al. (1978); Hoinkes et al. (1999); Schuster et al. (2001)). Cross section through the Schobergruppe and Prijakt eclogitic amphibolites **(d)** and through the Austroalpine basement to the south of Hopfgarten **(e)**. Sample locations and Th–U–Pb chemical ages of monazite are also shown

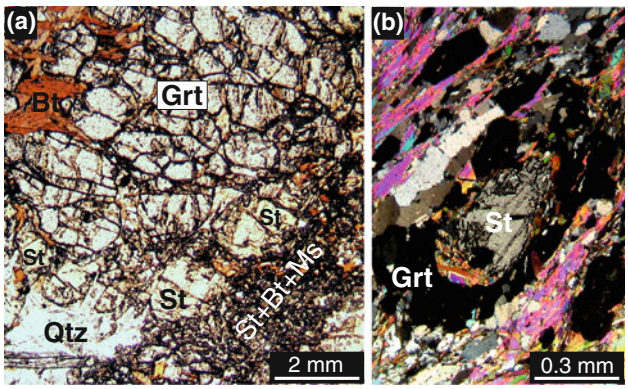

Fig. 2 Microphotographs showing garnet crystals associated with staurolite from sample 520 **(a)** and 527 **(b)**

in the vicinity of eclogitic amphibolites. The rocks are strongly foliated with modal abundances of approximately 5–10 vol. % garnet, 20–25 % quartz, 15–20 % plagioclase, 15–20 % muscovite, 10–15 % biotite, 3–5 % staurolite, 1–5 % chlorite and <3 % kyanite. Accessory phase are apatite, zircon, monazite and xenotime. The prevailing Ti-phase is ilmenite (0.5–2 vol. %).

Garnet is variable in size and shape, ranging from small (<300 μm) isometric, partly, rounded grains up to very large (several mm) eu- to subhedral crystals (Fig. 2). Under the microscope, garnet appears relatively homogeneous and not polyphase with little marginal breakdown and alteration. Inclusions of ilmenite, quartz, biotite, muscovite and plagioclase are common everywhere in the garnet. Garnet was also observed around staurolite (Fig. 2) or occurs intergrown with staurolite and/or mica-rich batches with remnants of staurolite (Fig. 2). Staurolite forms up to 5 mm large, eu- to subhedral crystals, sometimes twinned, sometimes elongated parallel to the foliation. In some places, staurolite occurs together with kyanite (see below). Kyanite is scarce and occurs as small grains or clusters (partly fibroblastic) associated with mica and/or staurolite.

Monazite from other garnet-bearing micaschists in this area was studied by Schulz et al. (2005, 2008). The corresponding samples were taken in the vicinity and below the eclogitic amphibolites to the south of the Oligocene Defereggen-Antholz-Vals shear zone (Fig. 1d, e). The samples were situated within and above a pegmatite-rich zone and within the monotonous metapsammopelitic Defereggen Group. The age of metamorphism remained unclear and the peak *P–T* conditions were considered pre-Alpine in age (Schulz et al. 2005, 2008). This is why we have revisited this area and resampled metapelites with zoned monazite as well as monazite inclusions in garnet, in order to establish correlations between monazite- and garnet growth stages.

4 Monazite

4.1 Chemical Th–U–Pb monazite dates

Backscattered electron imaging (BSE), phase identification with an energy-dispersive system (EDS) as well as dating and chemical analyses using the wavelength-dispersive system (WDS) were carried out with a JEOL-JX8600 electron microprobe following the procedures described in Krenn et al. (2008) and Krenn and Finger (2004). Single monazite dates and weighted average ages (Table 1) were calculated utilizing the method of Montel et al. (1996) and isoplot 2.1 (Ludwig 2001) considering the analytical 2 sigma errors on Th, U and Pb measurements. The analytical Pb-errors range from 0.010 to 0.016 for a Pb dwell time of 160–400 s.

The statistical distribution of measured monazite ages shows three peaks corresponding to Carboniferous (Variscan), Permian and Cretaceous (Eo-Alpine) times, respectively (Fig. 3). Data cluster around 300–330, 250–280 and 70–135 Ma, respectively, whereas a few dates between 220 and 250 Ma and ~300 Ma are interpreted as a mixture of ages due to the polyphase nature of monazite (see below). The weighted average dates per sample are listed in Table 1. In the Th* versus total-Pb diagram after Suzuki et al. (1991), pre-Alpine and Alpine monazite analyses arrange themselves along three trendlines (Fig. 4), which provide isochron ages of 321 ± 14 Ma, 261 ± 18 Ma and 112 ± 22 Ma, respectively. The Variscan trendline is characterized by a slope of 0.01429x (±0.0006x), an interception value of ~0 and a MSWD value of 0.4; the Permian regression defines a slope of 0.0117x (±0.0008x), an intercept value of ±0.0007 and a MSWD value of 0.3 and the Alpine trendline has a slope of 0.0055x (±0.0013x), an intercept value of 0.001 and a MSWD value of 0.24.

Variscan, Permian and/or Eo-Alpine (Cretaceous) monazite were also observed in other samples from the Schobergruppe and from the Defereggen Group, south to the DAV (Schulz et al. 2005, 2008). Sample HPr10 shows Permian and abundant Cretaceous monazite ages (Fig. 1b, d; Table 2), samples Alk2, Sti14 and P24 preferentially Permian ages and samples Alk 8, 839, 431b and 750b Variscan (Carboniferous) monazite ages (Fig. 1d, e; Table 2). It is important to note that it was beyond the scope of these earlier studies to analyze all monazite grains in a sample. Therefore, it is likely that other monazite

Table 1 Th, U, Pb concentration, Th* values, ages and 2 sigma errors of monazites

Sample	Site	Th	U	Pb	Th*	Age	$\pm 2\sigma$ (Ma)
Variscan monazite ages							
520	Matrix	2.146	0.648	0.073	4.262	382	55
520	Matrix	1.807	0.582	0.057	3.701	343	63
520	Grt rim	15.494	0.561	0.258	17.318	333	13
520	Matrix	0.710	0.343	0.028	1.826	341	128
520	Grt rim	13.557	0.601	0.238	15.514	344	18
520	Grt rim	14.343	0.582	0.225	16.231	310	18
520	Grt rim	3.125	0.839	0.079	5.847	304	40
520	Grt rim	1.527	0.756	0.060	3.986	338	59
520	Grt rim	3.610	0.890	0.089	6.499	308	36
520	Matrix	10.192	0.486	0.160	11.768	305	20
520	Matrix	2.904	0.855	0.079	5.679	313	41
520	Matrix	11.916	0.561	0.191	13.738	311	17
520	Matrix	3.130	0.768	0.081	5.627	322	41
520	Matrix	9.883	0.537	0.157	11.626	302	20
520	Matrix	11.778	0.535	0.189	13.517	313	21
520	Matrix	9.347	0.565	0.167	11.183	334	21
520	Matrix	3.359	0.842	0.082	6.090	303	38
520	Matrix	3.269	0.961	0.096	6.395	339	36
520	Matrix	3.393	0.832	0.090	6.099	331	38
520	Grt rim	14.329	0.546	0.220	16.101	307	18
Weighted average age						319	10
527	Grt rim	13.190	0.510	0.205	14.844	310	19
527	Grt rim	1.253	0.702	0.050	3.533	315	66
527	Grt rim	12.684	0.482	0.193	14.247	303	20
527	Matrix	11.043	0.439	0.184	12.470	331	23
527	Matrix	12.497	0.481	0.204	14.060	324	20
527	Matrix	11.712	0.422	0.193	13.083	330	18
527	Matrix	11.971	0.440	0.196	13.401	327	21
527	Grt rim	1.735	0.749	0.056	4.165	301	56
527	Grt rim	1.288	0.695	0.051	3.547	321	66
527	Matrix	12.417	0.497	0.205	14.034	328	20
527	Grt rim	11.389	0.518	0.190	13.073	325	18
527	Grt rim	11.333	0.542	0.184	13.093	314	18
527	Grt rim	10.131	0.501	0.174	11.759	331	20
527	Matrix	11.123	0.445	0.174	12.569	311	19
527	Grt rim	2.132	0.803	0.065	4.737	306	49
527	Grt rim	11.980	0.434	0.203	13.392	340	21
Weighted average age						322	9
Alk 8	Grt rim	8.492	0.490	0.153	10.085	339	23
Alk 8	Grt rim	7.140	0.501	0.122	8.768	311	27
Alk 8	Grt rim	5.096	0.682	0.106	7.311	324	32
Alk 8	Grt rim	4.422	0.737	0.093	6.812	305	34
Alk 8	Grt rim	3.326	0.770	0.080	5.826	307	40
Alk 8	Grt rim	8.630	0.522	0.139	10.323	303	23
Alk 8	Grt rim	10.079	0.566	0.174	11.918	327	20
Alk 8	Matrix	3.484	0.882	0.090	6.349	317	37
Alk 8	Matrix	3.627	0.938	0.101	6.680	338	35
Alk 8	Matrix	3.651	0.461	0.071	5.147	311	45
Alk 8	Matrix	9.873	0.557	0.172	11.683	330	20
Alk 8	Matrix	3.988	0.475	0.084	5.534	341	42
Alk 8	Matrix	3.463	0.945	0.088	6.530	302	36
Alk 8	Matrix	9.755	0.549	0.156	11.537	302	20
Alk 8	Matrix	9.795	0.501	0.158	11.422	310	20
Alk 8	Grt rim	1.591	0.670	0.056	3.771	332	62
Weighted average age						318	10
Permian monazite ages							
520	cracks	8.854	0.419	0.109	10.206	239	23
520	Grt rim	1.453	0.528	0.037	3.160	262	52
520	Matix	5.978	2.277	0.154	13.343	260	18
520	Matix	5.256	2.596	0.171	13.668	281	21
520	Matix	4.014	0.474	0.070	5.550	282	42
520	Grt rim	1.759	0.522	0.037	3.446	244	68
520	Matix	5.734	2.302	0.140	13.168	240	22
520	Grt rim	1.729	0.475	0.036	3.262	245	72
520	Matrix	3.854	0.824	0.076	6.519	264	36
520	cracks	6.297	0.408	0.086	7.615	254	31
520	cracks	9.067	0.514	0.118	10.727	246	22
520	Grt rim	0.513	1.080	0.048	4.010	270	59
520	Grt rim	0.473	0.785	0.035	3.012	264	78
520	St	3.336	0.443	0.063	4.772	296	49
520	St	1.894	0.386	0.040	3.146	286	74
520	St	1.912	0.323	0.036	2.958	272	79
520	St	2.111	0.313	0.035	3.121	251	75
520	St	2.074	0.302	0.035	3.051	256	77
520	Matrix	6.693	0.291	0.089	7.633	261	31
520	Grt rim	6.746	0.334	0.093	7.826	266	30
520	Matrix	6.594	0.360	0.098	7.759	282	30
Weighted average age						260	9
527	Matrix	1.393	1.027	0.060	4.720	285	50
527	Matrix	1.673	1.031	0.066	5.017	294	47
527	Matrix	0.987	0.577	0.029	2.850	230	82
527	Matrix	1.469	0.975	0.054	4.622	261	51
527	Matrix	1.112	1.170	0.052	4.891	238	48
527	Matrix	1.102	1.228	0.064	5.081	283	46
527	Matrix	0.936	1.158	0.051	4.677	248	50
527	Grt rim	5.006	0.722	0.082	7.338	250	32
527	Grt rim	4.912	0.787	0.080	7.455	240	31
527	Grt rim	5.060	0.796	0.101	7.640	297	31
527	Grt rim	3.098	0.882	0.074	5.955	281	39
527	Grt rim	3.058	0.904	0.072	5.982	269	39
527	Grt rim	3.905	0.682	0.064	6.107	236	38
527	Grt rim	3.177	0.400	0.053	4.472	264	52
527	Grt rim	3.270	0.439	0.052	4.688	249	50
527	Matrix	4.057	0.856	0.086	6.830	283	34
527	Matrix	3.508	0.752	0.075	5.946	284	39

Table 1 continued

Sample	Site	Th	U	Pb	Th*	Age	$\pm 2\sigma$ (Ma)
527	Matrix	3.747	0.978	0.090	6.916	291	34
527	Matrix	4.083	0.868	0.086	6.895	280	34
527	Matrix	3.217	0.739	0.069	5.611	277	42
527	Matrix	3.919	0.738	0.065	6.300	232	37
527	Matrix	4.325	0.800	0.078	6.912	252	34
527	Matrix	4.379	0.856	0.079	7.144	247	33
Weighted average age						265	10
Alk 8	Grt rim	4.645	0.985	0.087	7.827	250	30
Alk 8	Grt rim	4.832	0.969	0.097	7.968	275	29
Alk 8	Grt rim	4.547	0.932	0.081	7.558	242	31
Alk 8	Grt rim	11.133	0.288	0.146	12.066	271	19
Alk 8	Grt rim	5.715	0.391	0.089	6.982	285	33
Alk 8	Grt rim	5.462	0.413	0.081	6.798	266	34
Alk 8	Grt rim	6.183	0.486	0.081	7.752	234	30
Alk 8	Grt rim	5.789	0.511	0.095	7.444	285	31
Alk 8	Grtcore	1.308	0.437	0.031	2.721	256	86
Alk 8	St	2.363	0.437	0.040	3.774	238	62
Alk 8	Matrix	1.839	0.666	0.049	3.995	276	59
Alk 8	Matrix	1.892	0.646	0.043	3.978	242	59
Alk 8	Matrix	2.154	0.659	0.049	4.286	257	42
Weighted average age						263	10
Alpine monazite ages							
520	Matrix	3.729	1.296	0.039	7.875	110	26
520	Matrix	3.762	1.165	0.025	7.480	77	27
520	Matrix	3.720	1.277	0.034	7.804	98	26
520	Matrix	3.878	1.276	0.045	7.965	127	26
520	Grt rim	4.765	0.865	0.040	7.533	119	27
520	Grt rim	4.270	1.111	0.042	7.828	122	26
527	Grtcore	0.925	0.937	0.017	3.919	101	52
527	Grtcore	0.988	1.074	0.020	4.422	103	46
527	Matrix	0.919	0.935	0.021	3.912	120	52
Alk 8	Matrix	2.675	0.382	0.021	3.897	119	52
Alk 8	Matrix	3.111	0.389	0.019	4.353	96	47
Weighted average age						109	13

Th, U and Pb in wt % element;weighted average ages calculated with isoplot 2.1 (Ludwig 2001)

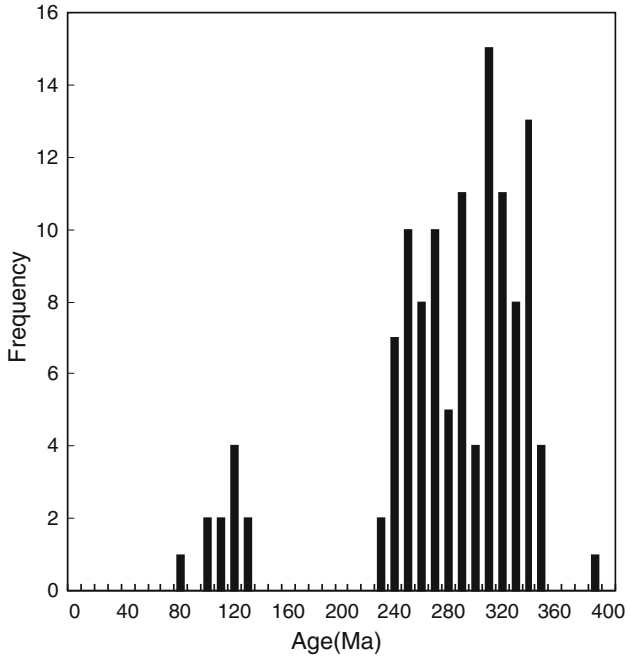

Fig. 3 Frequency diagram of monazite ages in samples 520, 527 and Alk 8

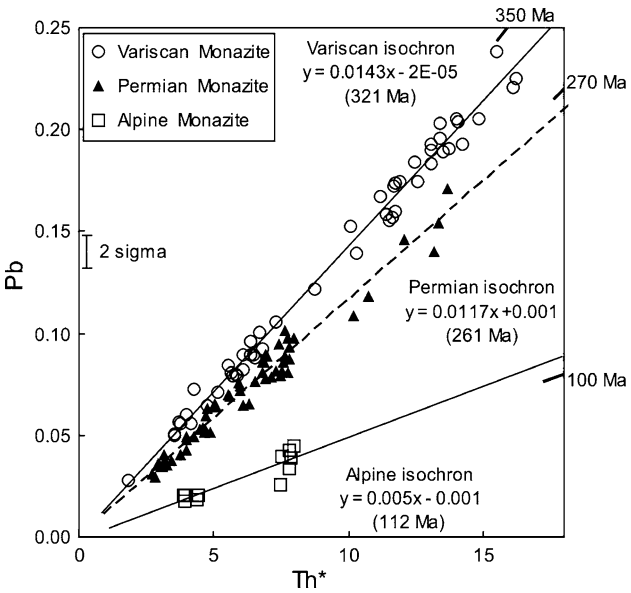

Fig. 4 Th* vs. Pb diagram after Suzuki et al. (1991) showing the trendlines defined through Alpine, Permian and Variscan monazite. Age bars on the right site are isochrones forced through 0

generations would be found as well if studied in more detail and the absence of a monazite age in these samples should not be over- or misinterpreted.

4.2 Morphology and chemistry of monazite

In all three samples investigated in this work, Variscan and Permian monazite form morphologically indistinguishable, relatively large eu- to subhedral grains (ca. 20–150 µm) (Fig. 5a, b). Some crystals show straight grain boundaries, others are irregular and embayed (Fig. 5b, c). Monazite grains were observed in the matrix as well as inclusions in staurolite and in the outermost domains of large garnet crystals (Fig. 5a), but not in the cores of the latter.

Approximately 1/3–1/2 of all monazite grains display a characteristic zoning in BSE images with bright cores (enriched in thorium; up to 16 wt. % ThO_2) and darker rims with lower Th contents (Table 3). Dating of these rim zones revealed that most of them are Permian in age,

Table 2 Th-U–Pb CHIME model ages of monazite from other garnet-bearing mica schists from the Schobergruppe and adjacent Austroalpine basement, as reported in Schulz et al. (2005)

Sample	Geological unit	Figure	Age (Ma)
HPr 10	Schobergruppe	1b, d	264 ± 14
HPr 10	Schobergruppe	1b, d	89 ± 6
HPr 8	Schobergruppe	1b, d	313 ± 35
Alk 2	Schobergruppe	1b, d	268 ± 8
Sti 14	Defereggengruppe	1b, e	276 ± 18
P 24	Defereggengruppe	1b, e	271 ± 15
839	Defereggengruppe	1b, e	307 ± 15
431b	Defereggengruppe	1b, e	309 ± 9
750b	Defereggengruppe	1b, e	308 ± 12

although both Variscan and Permian rims were locally observed (Fig. 5c). In Fig. 5c, a bright Th-rich Variscan core is surrounded by an optically darker Variscan rim, which in turn is followed by an outermost Permian rim (Fig. 5c; Table 3). Variscan domains (cores and rims) are low in Y (<1 wt. % Y_2O_3), while Y_2O_3 values in Permian rims are systematically (0.5–1.5 wt. %) higher than in the corresponding Variscan core (Table 3). In average, Variscan monazite shows higher Th- and lower Y contents than Permian monazite (3–16 wt. % ThO_2 and 0.1–1wt. % Y_2O_3 vs. 1–8 wt. % ThO_2 and 0.2–2.5 wt. % Y_2O_3; Figs. 6, 7). In addition, Variscan monazite provides a slight positive covariation between Th and Y, while Th and Y in Permian monazite are negatively correlated or not correlated at all (Fig. 7).

Eo-Alpine monazite occurs in small and unzoned grains (<10 µm), which, in some places, arrange themselves in clusters (Fig. 5f, g). Monazite in sample Alk8 was only observed in the matrix, while monazite in samples 520 and 527 was found in the matrix as well as enclosed in small, optically homogeneous and widely unaltered garnet crystals (Fig. 5f, g). Eo-Alpine monazite is not texturally associated with allanite (as is in sample HPr10 from Schulz et al. 2005, 2008) or with pre-Alpine monazite, but was found together with or nearby xenotime (Fig. 5h). Eo-Alpine monazite yields ca. 1.5–6 wt. % ThO_2 and shows a considerable Y-variation from ca. 1 wt. % Y_2O_3 (as is the case for monazite in garnet) up to 2.9 wt. % Y_2O_3 (Fig. 6; Table 3). The highest Y-values were observed in a matrix

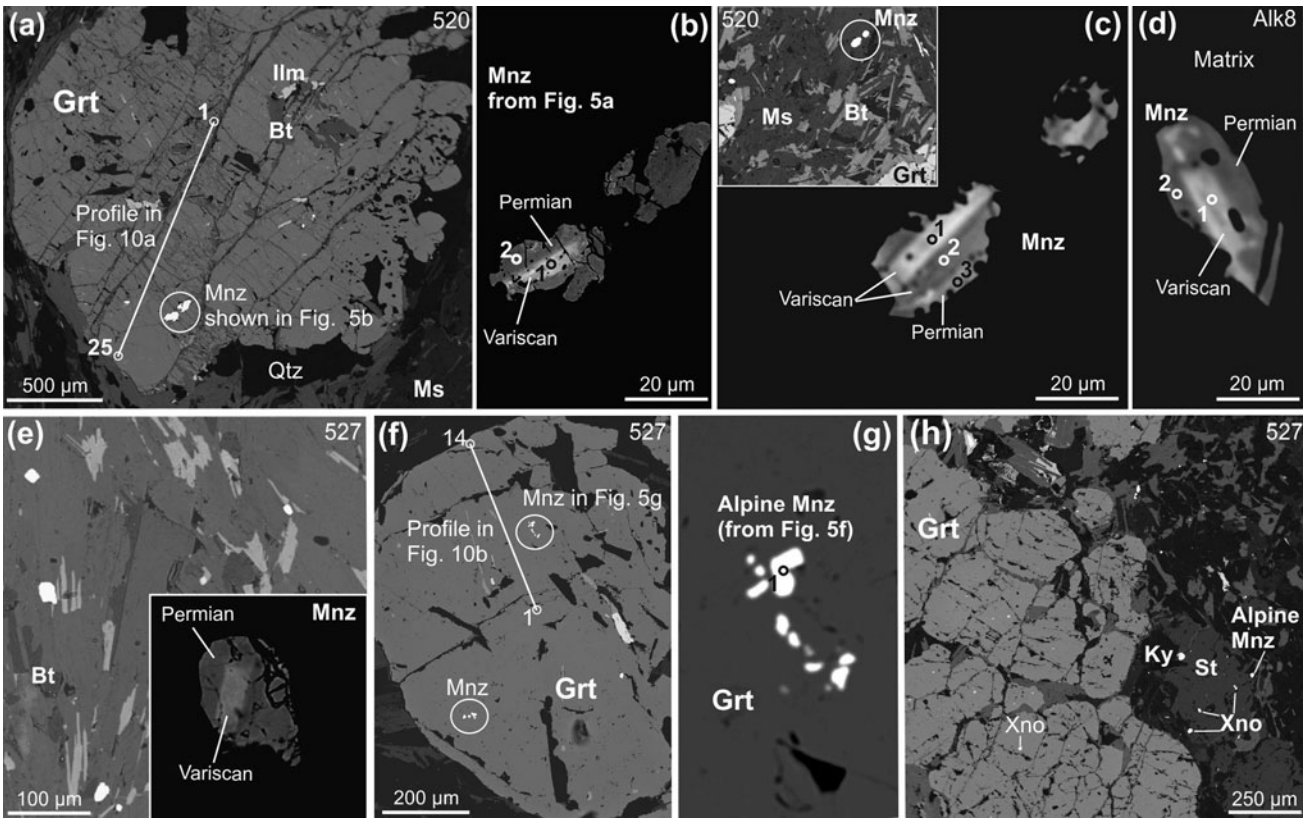

Fig. 5 Backscattered electron images showing monazite from samples 520, 527 and Alk 8. Polyphase monazite (Variscan core, Permian rim) enclosed in the outer domain of garnet **(a, b)**. Polyphase matrix monazite with a Variscan core (labeled as analysis 1), Variscan rim (analysis 2) and an outermost Permian rim (analysis 3) **(c)**. Polyphase matrix monazite with a Variscan core and Permian rim **(d, e)**. Alpine monazite enclosed in garnet. **(h)** Alpine monazite in the staurolite-kyanite bearing matrix **(f, g)**. Chemistry and ages of monazite are listed in Tables 1, 2, 3, and garnet compositions are shown in Figs. 10 and 11

Table 3 Selected microprobe analyses of monazites

	Fig. 4b/1	Fig. 4b/2	Fig. 4c/1	Fig. 4c/2	Fig. 4c/3	Fig. 4d/1	Fig. 4d/2	Fig. 4g
wt %								
SiO_2	1.41	0.12	0.84	0.05	0.59	0.86	0.10	0.05
Al_2O_3	<d.l.	<d.l.	<d.l.	<d.l.	<d.l.	<d.l.	<d.l.	<d.l.
P_2O_5	28.10	29.92	29.79	29.73	28.16	29.47	29.18	29.28
CaO	2.38	0.49	1.99	1.04	1.38	2.04	0.68	0.47
Y_2O_3	0.93	1.33	0.53	0.26	1.26	0.80	0.49	1.92
La_2O_3	10.49	13.82	11.91	13.69	12.55	11.38	14.15	13.67
Ce_2O_3	23.01	31.43	26.99	30.39	27.18	25.13	31.24	31.10
Pr_2O_3	2.56	3.13	2.75	3.20	2.93	2.71	3.18	3.05
Nd_2O_3	9.39	12.65	10.68	12.61	11.85	10.30	12.07	12.39
Sm_2O_3	2.02	2.21	1.93	2.16	1.95	1.90	2.20	2.17
Gd_2O_3	1.91	1.55	1.66	1.42	1.45	1.74	1.36	1.41
Dy_2O_3	0.45	0.46	0.45	0.19	0.60	0.37	0.21	0.37
Er_2O_3	0.08	0.12	<d.l.	0.09	0.12	<d.l.	<d.l.	0.24
Yb_2O_3	<d.l.	<d.l.	<d.l.	<d.l.	<d.l.	<d.l.	<d.l.	<d.l.
ThO_2	15.43	1.65	10.64	3.86	7.68	11.23	2.45	1.05
UO_2	0.68	0.60	0.64	0.94	0.38	0.63	0.75	1.06
PbO	0.26	0.04	0.18	0.10	0.10	0.19	0.05	0.02
Sum	99.09	99.54	101.04	99.73	98.17	98.75	98.12	98.24
a.p.f.u								
Si	0.056	0.005	0.033	0.002	0.024	0.034	0.004	0.002
P	0.951	0.995	0.978	0.994	0.965	0.984	0.992	0.990
Ca	0.102	0.021	0.083	0.044	0.060	0.086	0.029	0.020
Y	0.020	0.028	0.011	0.005	0.027	0.017	0.010	0.041
La	0.155	0.200	0.170	0.199	0.187	0.165	0.210	0.201
Ce	0.337	0.452	0.383	0.439	0.403	0.363	0.459	0.455
Pr	0.037	0.045	0.039	0.046	0.043	0.039	0.046	0.044
Nd	0.134	0.178	0.148	0.178	0.171	0.145	0.173	0.177
Sm	0.028	0.030	0.026	0.029	0.027	0.026	0.030	0.030
Gd	0.025	0.020	0.021	0.019	0.019	0.023	0.018	0.019
Dy	0.006	0.006	0.006	0.002	0.008	0.005	0.003	0.005
Er	0.001	0.001	–	0.001	0.002	–	–	0.003
Yb	–	–	–	–	–	–	–	–
Th	0.140	0.015	0.094	0.035	0.071	0.101	0.022	0.010
U	0.006	0.005	0.006	0.008	0.003	0.006	0.007	0.009
Pb	0.003	0.000	0.002	0.001	0.001	0.002	0.001	0.000
Tetr.	1.007	1.000	1.011	0.996	0.989	1.017	0.996	0.992
Pol.	0.993	1.002	0.988	1.008	1.023	0.976	1.009	1.014
Age	344	262	334	331	266	330	257	101
	±	±	±	±	±	±	±	±
Error	18	52	21	38	29	20	42	51

at the boundary of staurolite-kyanite-muscovite aggregates and in the close vicinity to xenotime crystals (Fig. 5). Xenotime is common in all samples and occurs as small grains or in clusters in the matrix and enclosed in garnet (see below).

4.3 Monazite-xenotime thermometry

Minimum growth temperatures of monazite were obtained utilizing monazite-xenotime miscibility gap thermometers. Figure 8 shows the experimentally calibrated 2 kbar

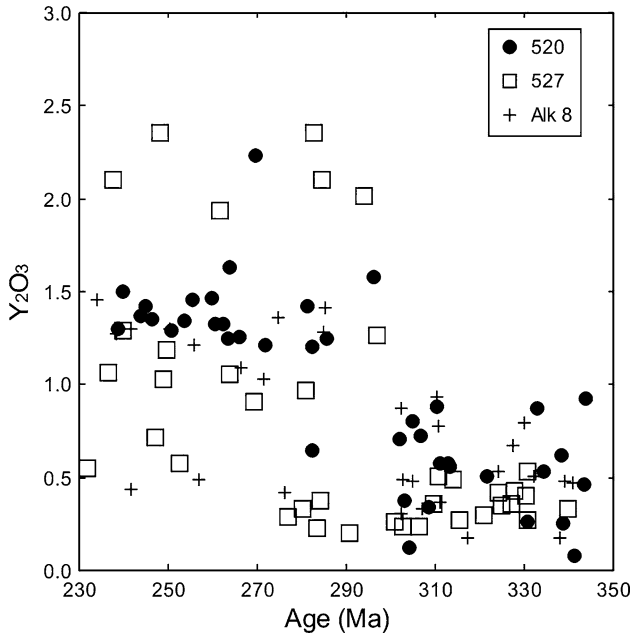

Fig. 6 Th versus Y trends of Variscan, Permian and Alpine monazite

thermometer curve of Gratz and Heinrich (1997), the empirical thermometer of Heinrich et al. (1997), which was obtained on low-pressure rocks and the empirical thermometer of Pyle et al. (2001) calibrated on high pressure rocks. Also shown is the experimentally 2 kbar curve for huttonite-bearing monazite with ca. 10 % huttonite (Seydoux-Guillaume et al. 2002). This thermometer curve runs sub-parallel to the 2 kbar curve of Gratz and Heinrich (1997) at ca. 30–50 °C lower temperatures. The Gratz and Heinrich (1997) thermometer was calibrated in the binary $CePO_4$–YPO_4 system disregarding the stronger Y-uptake of huttonite-bearing monazite.

The highest xenotime value observed in Permian monazite (~8 mol %) intersects the low-pressure curves of Heinrich et al. (1997); Gratz and Heinrich (1997) and Seydoux-Guillaume et al. (2002) between ca. 650 and 700 °C (Fig. 8). The highest xenotime value observed in Eo-Alpine monazite (ca. 10 mol %) intersects the thermometer curve of Pyle et al. (2001) at temperatures of ca. 650 °C, those calibrated for low-pressure rocks at ~700 °C. Maximum

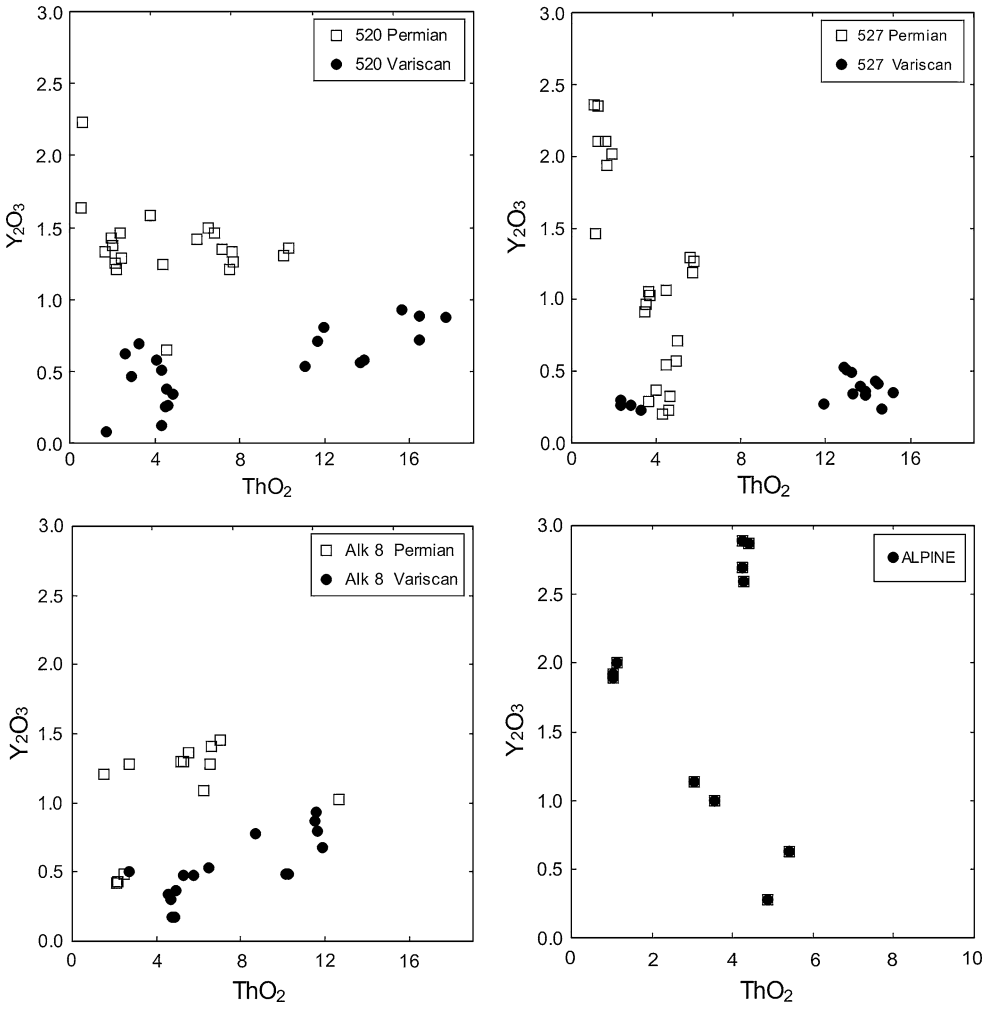

Fig. 7 Chemical composition of Variscan and Permian monazite

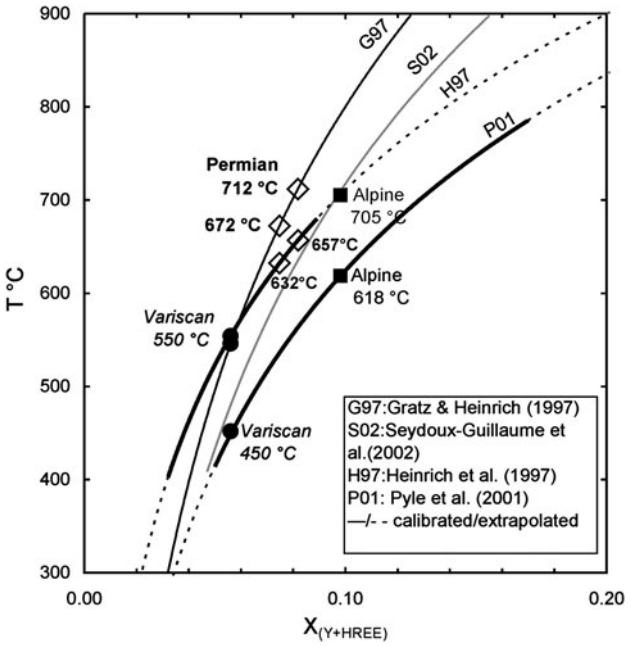

Fig. 8 Xenotime versus temperature diagram showing the published monazite-xenotime miscibility gap thermometer curves and the minimum formation temperatures of Variscan, Permian and Alpine monazite under study

xenotime contents observed in Variscan monazite (5 mol %) implies growth temperatures between 450 °C (Pyle et al. 2001) and 550 °C (Heinrich et al. 1997). Table 4 lists the (minimum) formation temperatures calculated utilizing the thermometer-functions given by Gratz and Heinrich (1997); Heinrich et al. (1997) and Pyle et al. (2001).

5 Major phase composition and geothermobarometry

Most garnet crystals, including those with inclusions of Eo-Alpine and Permian monazite (Fig. 5a, f) and those surrounding staurolite (Fig. 9b), show a simple core to rim zoning with a rimward decrease of MnO and CaO (1–0.1 wt. %; 3–0.1 wt. %) and increase of MgO (2.5–4 wt. %; Fig. 10). However, a few of the larger garnet crystals also yield a Mn-enriched core (plateau) with 3–4 wt. % MnO and 1–2 wt. % CaO and MgO (Fig. 11), followed by a rim domain, which is characterized by an abrupt decrease of MnO and increase of CaO and MgO (up to ca. 3–4 wt. %). The composition of the latter rims is similar to the garnet crystals shown in Fig. 10. A narrow retrogressive rim (max. 100–200 μm) is common in all investigated garnet grains.

Biotite is chemically homogeneous with a Mg/(Mg + Fe) of 0.4–0.5 and Ti contents from 1.5 to 2 wt % TiO_2, whether in the matrix or enclosed in garnet. Muscovite usually shows a weak diffuse zoning with slightly varying Na- and Ti values (1.3–2.5 wt. % Na_2O and 0.6–1.5 wt. % TiO_2). Plagioclase composition ranges from An_2 in the core to An_{12} at the rim.

An independent set of reactions obtained with the THERMOCALC software 3.21 (Holland and Powell 1998) yields *P–T* estimates of ca. 600–700 °C and 6–9 kbar for the assemblage biotite, muscovite, plagioclase-core and Mg-enriched garnet domains, and 550–600 °C and 14–16 kbar for the assemblage biotite, muscovite, plagioclase-rim and grossular-enriched garnet domains. We are aware that pressure estimates suffer from low An-contents of the plagioclase (e.g. Todd 1998). However similar *P–T* estimates of 650–700 °C/8–10 kbar and 550–650 °C/12–14 kbar were obtained by Schulz et al. (2005) for other low- and high-Ca metapelites from the Schobergruppe. These authors used the garnet-biotite thermometer of Bhattacharya et al. (1992) in combination with the garnet-muscovite-biotite-plagioclase barometer of Holland and Powell (1990) with updated activity models from Ganguly et al. (1996) and Powell and Holland (1993). The *P–T* estimates obtained from metapelites overlap with those obtained from eclogites and eclogitic amphibolites (Schulz 1993a; Schulz et al. 2008), which are intimately associated with the studied metapelites (see Fig. 1b and discussion below).

6 Discussion

6.1 Formation of pre-Alpine monazite

The occurrence of pre-Alpine monazite in the Schobergruppe samples is a clear evidence that parts of this area were pervasively metamorphosed during Variscan and Permian times. We conclude from the monazite-xenotime miscibility gap thermometry that the Variscan and Permian events reached temperatures of at least 500 and 650 °C, respectively (Fig. 8; Table 4). However, many Variscan monazite grains show xenotime contents of <5 mol % possibly because they crystallized at lower temperatures along the prograde Variscan metamorphic path or because they failed to attain maximum Y contents. Growth of monazite at temperatures much below 500 °C is not consistent with its high Th contents (up to 16 wt. % ThO_2) and with its large, euhedral crystals. Low-T monazite usually has much lower Th contents and/or its crystals are smaller and sub- to anhedral (e.g., Read et al. 1987; Rasmussen et al. 2001; Evans et al. 2002; Kryza et al. 2004; Wilby et al. 2007; Krenn et al. 2008; Del Rio et al. 2009; Bišević et al. 2011; Čopjaková et al. 2011). In addition monazite often occurs in greater abundances at upper greenschist to lower amphibolite facies conditions in many metapelitic

Table 4 Xenotime values of monazite and corresponding monazite-xenotime miscibility gap temperatures

Sample	Xno mol (%)	P01 T (°C)	H97 T (°C)	G97 T (°C)	Sample	Xno mol (%)	P01 T (°C)	H97 T (°C)	G97 T (°C)
Variscan Mnz					Permian Mnz				
520	0.03	282	400	296	520	0.06	482	582	590
520	0.03	265	385	271	520	0.07	505	602	624
520	0.05	394	502	461	520	0.07	500	597	616
520	0.04	383	492	444	520	0.04	345	458	389
520	0.05	428	533	511	520	0.06	468	569	570
520	0.06	452	554	546	520	0.06	448	551	540
520	0.02	163	293	122	520	0.06	458	560	555
520	0.04	331	444	368	520	0.06	453	555	548
520	0.02	197	323	171	520	0.07	511	608	633
520	0.01	–	119	–	520	0.07	523	618	650
520	0.04	364	475	417	520	0.07	538	632	672
520	0.04	323	437	356	520	0.08	565	657	712
520	0.04	383	492	445	520	0.06	491	589	603
520	0.05	397	505	466	520	0.06	468	568	569
520	0.04	350	462	396	520	0.05	442	546	532
520	0.04	338	451	379	520	0.06	467	568	568
520	0.04	339	452	381	520	0.06	451	553	544
520	0.03	216	341	200	520	0.06	473	573	577
520	0.03	242	364	238	520	0.05	417	522	494
520	0.03	240	362	235	520	0.06	451	553	544
527	0.03	233	356	225	520	0.06	465	567	566
527	0.02	196	322	170					
527	0.02	90	227	15	527	0.08	554	646	695
527	0.03	299	416	321	527	0.07	526	621	654
527	0.04	344	456	387	527	0.06	461	562	559
527	0.03	239	361	233	527	0.07	528	623	658
527	0.03	229	352	219	527	0.08	543	636	679
527	0.03	247	369	246	527	0.08	566	658	714
527	0.03	262	382	267	527	0.08	553	646	695
527	0.03	275	394	286	527	0.05	428	533	511
527	0.04	313	428	342	527	0.06	453	555	547
527	0.03	252	373	253	527	0.06	447	550	539
527	0.02	181	309	149	527	0.05	402	509	472
527	0.03	210	335	191	527	0.04	384	493	446
527	0.03	238	361	233	527	0.05	386	495	450
527	0.03	211	336	192	527	0.05	388	497	453
Alk 8	0.06	447	550	539	527	0.04	372	482	429
Alk 8	0.03	308	424	335	527	0.02	166	295	126
Alk 8	0.03	304	420	329	527	0.03	266	385	273
Alk 8	0.03	297	414	318	527	0.02	175	303	139
Alk 8	0.03	293	410	313	527	0.03	225	349	214
Alk 8	0.04	366	476	419	527	0.02	196	322	170
Alk 8	0.03	255	376	257	527	0.03	296	413	318
Alk 8	0.02	150	281	103	527	0.03	275	394	286
Alk 8	0.02	179	307	145	527	0.04	327	442	363
Alk 8	0.04	322	437	355					
Alk 8	0.04	333	447	372	Alk 8	0.05	444	547	535

Table 4 continued

Sample	Xno mol (%)	P01 T (°C)	H97 T (°C)	G97 T (°C)	Sample	Xno mol (%)	P01 T (°C)	H97 T (°C)	G97 T (°C)
Alk 8	0.03	261	381	265	Alk 8	0.06	458	560	555
Alk 8	0.04	381	490	442	Alk 8	0.06	459	561	556
Alk 8	0.05	432	536	516	Alk 8	0.04	377	486	436
Alk 8	0.05	427	532	510	Alk 8	0.05	437	541	524
Alk 8	0.03	288	405	305	Alk 8	0.05	410	517	485
					Alk 8	0.05	429	533	512
Alpine monazite					Alk 8	0.05	420	526	500
520	0.09	592	681	751	Alk 8	0.05	434	538	520
520	0.09	594	683	755	Alk 8	0.06	464	565	564
520	0.10	619	705	791	Alk 8	0.03	274	393	285
520	0.09	606	694	773	Alk 8	0.03	267	386	274
520	0.03	281	400	295	Alk 8	0.03	277	396	289
520	0.03	229	353	219					
527	0.07	507	604	626					
527	0.07	535	630	669					
527	0.07	502	600	620					
Alk 8	0.05	425	529	506					
Alk 8	0.04	376	486	435					

P01 Pyle et al. (2001), *H97* Heinrich et al. (1997), *G97* Gratz and Heinrich (1997) *Mnz* Monazite

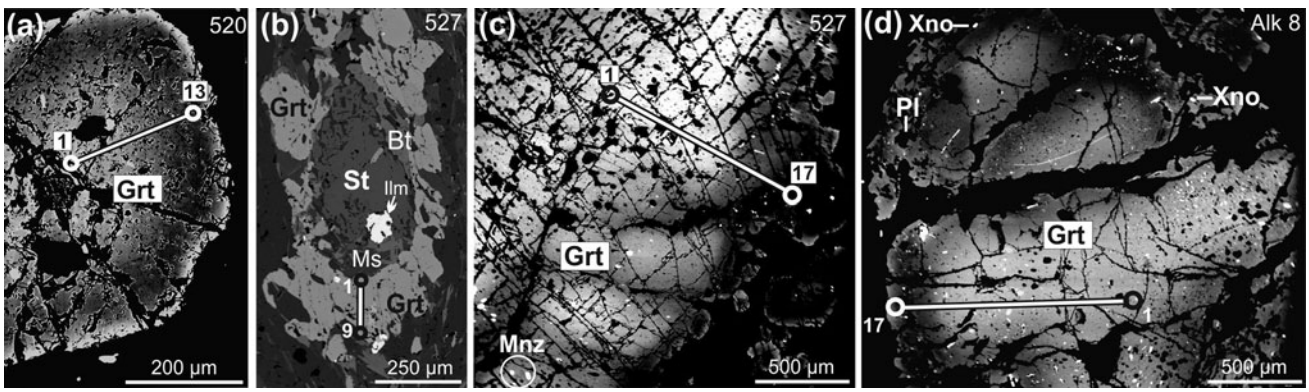

Fig. 9 Backscattered electron images of garnet from samples 520, 527 and Alk 8. Euhedral garnet with a simple zoning and a narrow alteration rim **(a)**. Garnet around staurolite shown in Fig. 2b **(b)**. Large garnet with diffuse zoning and inclusion of Permian monazite in its outer domains **(c)**. Large garnet with diffuse zoning and inclusion of xenotime. Chemical profiles are shown in Figs. 10 and 11**(d)**

rocks (Kingsbury et al. 1993; Lanzirotti and Hanson 1996; Wing et al. 2003).

It is likely that Variscan monazite with lower Y contents grew at a stage when Y was trapped in other phases like garnet. Garnet has indeed a high affinity for Y (Pyle and Spear 1999; Pyle et al. 2001) and this element will be less available for monazite if garnet growth occurs before monazite; alternatively, Y will be released and made available when garnet breaks down. Thus low Y contents in some Variscan monazite grains could be explained by its uptake in garnet porphyroblasts, which crystallized at Variscan times prior to monazite. Subsequent garnet resorption coupled to Y release, could be responsible for the much higher Y contents observed in Permian monazite (Fig. 7), which cannot come from the Variscan low-Y monazite generation alone. It is also likely that xenotime crystallized during this period of garnet resorption (e.g. Pyle et al. 2001). Possibly some of the xenotime grains observed within garnet formed together with Permian high-Y monazite.

The replacement of Variscan, low-Y monazite by Permian, high-Y monazite might be explained in terms of

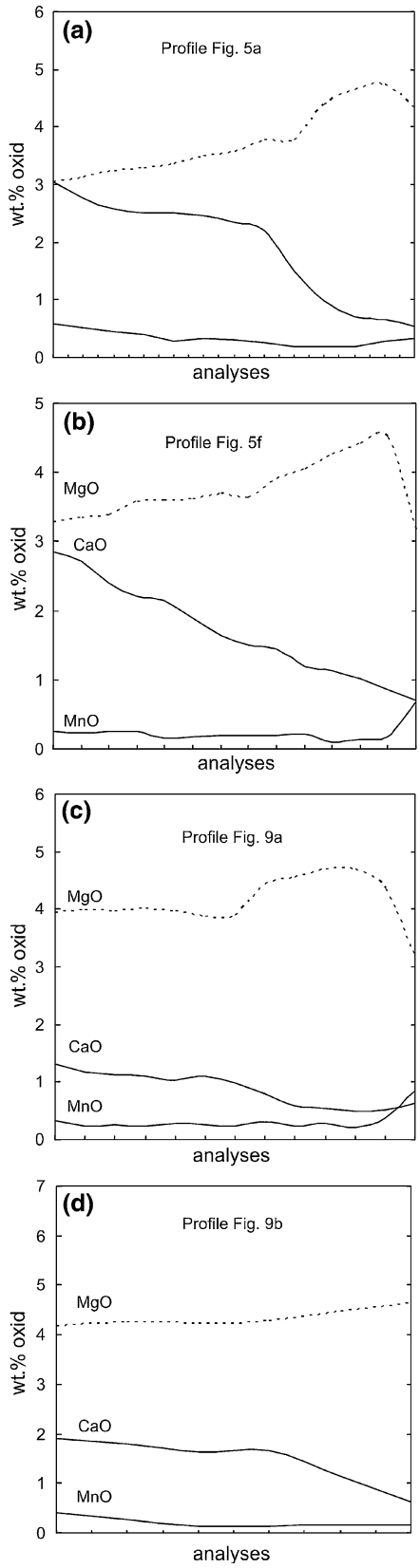

Fig. 10 Chemical composition of low Mn-garnet, shown in Figs. 5a, f and 9a, b

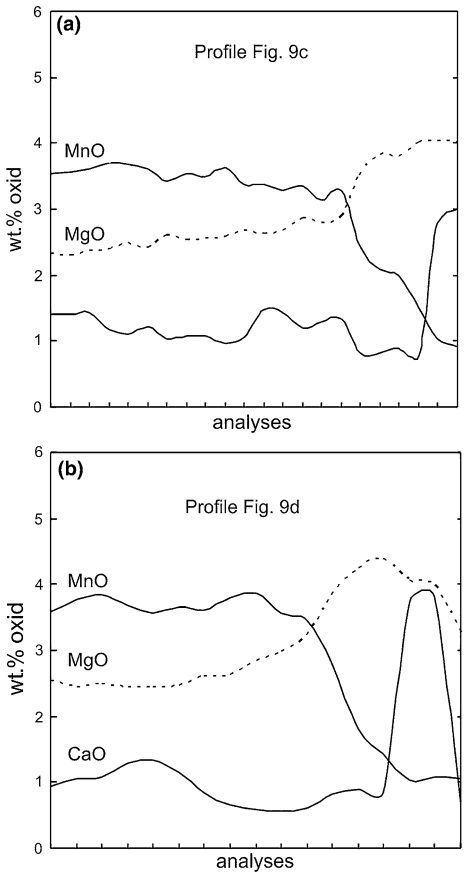

Fig. 11 Chemical composition of high Mn-garnet grains, shown in the Fig. 9c and d

dissolution and reprecipitation processes caused through the high temperatures and higher Y activity during the Permian event. Retrogression of the samples during the Permian coupled with liberation of Y could be a plausible explanation for the onset of abundant Permian monazite. Variscan low-Y monazite grains probably recrystallized in order to adjust their Y contents to the higher temperatures during the Permian event. This is a recrystallization mechanism that has been reported in other studies as well (e.g. Janots et al. 2008). A high strain rate (Berger et al. 2006) and a high degree of retrogression/alteration (Lanzirotti and Hanson 1996; Poitrasson et al. 1996, 2000; Krenn and Finger 2007; Budzyń et al. 2011) are also favorable for monazite recrystallization. Indentions and protrusions observed at the contacts between distinct monazite age zones (Fig. 5) suggest that pre-existing Variscan monazites were marginally replaced through a dissolution and reprecipitation mechanism (e.g. Putnis 2002, 2009). On the other hand, the euhedral shape of Variscan monazite cores also indicate that some of them were probably overgrown by neighboring monazite substance. This could be an explanation for the lower

Th-contents in some Permian monazite rims compared to the corresponding Variscan monazite cores.

6.2 Formation of Eo-Alpine monazite

Although monazite can survive high-grade metamorphism and even migmatite-grade conditions (e.g. Zhu and O'Nions 1999a, b; Martins et al. 2009), it is surprising that so many pre-Alpine monazite grains survived the Eo-Alpine amphibolite facies event. It is assumed that pre-Alpine monazites remained unaffected because their Y contents (at least in Permian monazite) were high and the degree of retrogression of the samples during the Eo-Alpine event was low. Krenn and Finger (2007) showed that the pre-existing Variscan monazite generation in polymetamorphic rocks from Crete remained largely unchanged in quartz-rich layers but barely survived in mica-rich layers of the same rock. The results showed that a lack of monazite age generation should not be misinterpreted as indicating that the degree of a metamorphic event was low or that a metamorphic event did not occur at all. Krenn and Finger (2007) also showed that the younger monazite generation likely formed in allanite-bearing domains, while allanite-absent domains hardly yielded young monazite. Indeed, in sample HPr10 from the Schobergruppe, where Eo-Alpine monazite is abundant (Schulz et al. 2005), allanite is common as well. It served as a direct precursor to Eo-Alpine monazite, as reported in other studies (e.g. Wing et al. 2003; Janots et al. 2006, 2008). No allanite formed in samples 520, 527 and Alk8, probably because of a low bulk Ca content, which is more favorable to the growth of monazite relative to that of allanite according to Janots et al. (2007) and Spear (2010). Allanite is often the prevailing REE-bearing phase in metapelites up to lower amphibolite facies conditions, where it reacts to monazite (e.g., Wing et al. 2003). The allanite to monazite transition has a slight positive slope in *P–T* space (Janots et al. 2007; Spear 2010) and moves towards lower temperatures with decreasing CaO whole-rock content or with increasing Al_2O_3 content. This results in a decrease or complete disappearance of the allanite stability field.

6.3 Growth of garnet

We identified three growth stages of garnet (M1–M3). M1 is observed sporadically in the cores of a few garnet crystals and is characterized by high Mn and low Mg values. M2 shows high Ca and intermediate Mg values and can be related to a high-pressure amphibolite facies stage at 550–600 °C/13–16 kbar. Garnet growth zone M3 prevails in many garnet crystals and is characterized by decreasing Ca and increasing Mg at low Mn contents resulting from a thermal maximum at 650–700 °C/6–9 kbar. The following assemblages (including quartz and muscovite) were observed together with the garnet growth zones M1–M3: M1 − garnet + chlorite; M2 − garnet + chlorite + biotite + plagioclase + monazite + xenotime ± staurolite ± kyanite; M3 − garnet + chlorite + biotite + plagioclase + staurolite + kyanite + monazite + xenotime. M2 and M3 stages were also documented in other micaschists from the Schobergruppe (Schulz et al. 2005, 2008) and match the thermobarometric results obtained from eclogitic amphibolites (Schulz 1993a; Schulz et al. 2008). Eclogitic amphibolites (Schulz 1993a; Schulz et al. 2008) contain a high-pressure assemblage of garnet plus clinopyroxene, which can be related to the M2 stage observed in metapelites and a subsequent high-temperature assemblage with Ca-amphibole plus zoisite, which can be ascribed to the M3 stage in metapelites. Eclogitic amphibolites are situated structurally below and above the micaschists with parallel planar-linear structures indicative of a common deformation history. *P–T* estimates for M2 and M3 are also in agreement with those obtained for other basement rocks from the Schobergruppe (Hoinkes et al. 1999; Linner et al. 2000).

However, while Hoinkes et al. (1999) ascribed the M2 and M3 stages to a Cretaceous event, Schulz (1993a) and Schulz et al. (2005, 2008) proposed a Variscan age. Results from this study, in particular the observation of Eo-Alpine monazite inclusions within M2 and M3 garnet domains, suggest that the M2 and M3 stages are Eo-Alpine rather than pre-Alpine. It is unlikely that the Eo-Alpine monazite grains shown in Fig. 5e crystallized after they were enclosed in garnet. There are no textural evidences such as pseudomorphs, recrystallization patches or overgrowths, which would argue for a later formation of monazite. Also, there are no cracks visible along which REEs could have entered garnet. In addition, REEs are relatively immobile during regional metamorphic processes and migration of REEs is expected rather at low metamorphic grade associated with diagenetic-, hydrothermal- and metasomatic processes (see Čopjaková et al. 2011 and references therein). Moreover, the high xenotime content observed in some Eo-Alpine monazite is also consistent with crystallization during the M3 thermal peak.

6.4 Pre-Alpine development of garnet

The age and growth conditions of M1-related garnet are not well known because they lack inclusions of biotite, plagioclase and monazite. Although we do not know if M1-related garnet domains represent pre-Alpine remnants, this is likely for several reasons. According to the monazite thermometry, samples 520, 527, Alk 8a were metamorphosed at temperatures of 500 and 650 °C during the Variscan and Permian events, respectively. This is high enough for the growth of garnet. In addition, growth of

Variscan and Permian garnet has been documented from other metapelitic samples from the basement south of the Tauern window (Schuster et al. 2001; Steidl et al. 2010a, b). Steidl et al. (2010a, b) proposed *P–T* conditions of 3.8–5.8 kbar and up to 650 °C for the Permian event and assumed amphibolite facies conditions for the Variscan event. Similarly our results would argue for a high-temperature Permian event and a Variscan event at lower amphibolite facies conditions.

According to the structural position of some of the studied metapelites (Fig. 1b, d), Permian recrystallization in these rocks may be related to the intrusion of Permian pegmatites. However, Permian monazite in other metapelites, which occur at a greater distance to pegmatites (Fig. 1), would rather argue for a discrete Permian *HT/LP* event. This is supposed by Schuster and Stüwe (2008) for the metamorphic complexes south and southeast of the Schobergruppe (Jenig and Strieden Complexes). Moreover, the large number of pegmatites across the entire basement of the Schobergruppe (Bücksteeg 1999) is also consistent with a regional Permian *HT/LP* event (Schuster and Stüwe 2008), which would have been accompanied by partial melting of the lower crust.

Permian metamorphism is widespread in the Eastern Alps (Habler and Thöni 2001; Schuster et al. 2001) and is particularly pronounced in the crystalline complexes of the so-called Wölz-Koralpe nappe system (Schuster et al. 2004). Remnants of Variscan mineral assemblages are rarely observed in rocks from the Wölz-Koralpe nappe system and have been reported for instance from the Strieden and Jenig Complexes (Schuster et al. 2001, 2004), the Michelbach Complex of the Defereggen Mountains (Steidl et al. 2010a, b) or from the Rappold Complex (Gaidies et al. 2008). From these units, the Rappold Complex shows a similarly high-grade metamorphic Eo-Alpine overprint (Gaidies et al. 2008) like the studied samples from the Schobergruppe. Other crystalline complexes of the Wölz-Koralpe nappe system (e.g., Wölz Unit, Saualpe-Koralpe Complexes, Pohorjeh Mountains, Schneeberg Complex) usually contain assemblages indicative for a Permian and/or a Eo-Alpine imprint (e.g., Abart and Martinelli 1991; Schuster and Thöni 1996; Thöni and Miller 1996; Bernhard and Hoinkes 1999; Faryad and Chakraborty 2005; Gaidies et al. 2006; 2008; Schuster et al. 2001).

7 Conclusions

Petrographic and textural evidence from different generations of monazite crystals indicate a Cretaceous Eo-Alpine age for the high-pressure amphibolite facies metamorphic events M2 and M3 recorded in the Schobergruppe. In contrast, relict monazite crystals record pre-Alpine metamorphic events of amphibolite grade, whatever the intensity of the subsequent Alpine overprint. Monazite records Carboniferous, Permian and Cretaceous age groups in agreement with preexisting data in the Schobergruppe, like sample HPr10, which documents a distinct Cretaceous monazite crystallization event in the lower parts of the Northern-Defereggen-Petzeck Group. The finding of Permian monazite ages in samples with both multi and single monazite age populations implies a metamorphism event clearly distinct from those of Variscan and Alpine ages. This study also illustrates the resistance of monazite at very high-grade metamorphic conditions and its potential use as a relict in unraveling the complex history of polymetamorphic rocks.

Acknowledgments This work was supported by the Austrian Science Foundation through projects P13070 and P22408 (to F.F.) and by the Deutsche Forschungsgemeinschaft (Project SCHU-676-9). M. Göbbels and N. Langhof are thanked for their assistance during electron-microprobe sessions and François Bussy for handling the manuscript. The work strongly benefited from thorough reviews of Alfons Berger and Peter Tropper.

References

Abart, R., & Martinelli, W. (1991). Variszische und alpidische Entwicklungsgeschichte des Wölzer Kristallins (Steiermark, Österreich). *Mitteilungen der Gesellschaft der Geologie- und Bergbaustudenten in Österreich, 37*, 1–14.

Berger, A., Herwegh, M., & Gnos, E. (2006). Deformation of monazite in an amphibolite-facies shear zone. *Geochimica et Cosmochimica Acta, 70*, A47–A47.

Bernhard, F., & Hoinkes, G. (1999). Polyphase micaschists of the central Wölzer Tauern, Styria, Austria. *Berichte der Deutschen Mineralogischen Gesellschaft, Beiheft zum European Journal of Mineralogy, 11*, 32.

Bhattacharya, A., Mohanty, L., Maji, A., Sen, S. K., & Raith, M. (1992). Non-ideal mixing in the phlogopite-annite binary: constraints from experimental data on Fe-Mg partitioning and a reformulation of the garnet-biotite geothermometer. *Contributions to Mineralogy and Petrology, 111*, 87–93.

Biševac, V., Krenn, E., Balen, D., Finger, F., & Balogh, K. (2011). Petrographic, geochemical and geo-chronological investigations on granitic pebbles from Permotriassic metasediments of the Tisia terrane (eastern Papuk, Croatia). *Mineralogy and Petrology, 102*, 163–180.

Borsi, S., Del Moro, A., Sassi, F. P., Zanferrari, A., Zirpoli, G. (1978). New geopetrologic and radiome-tric data on the Alpine history of the Austridic continental margin south of the Tauern Window. *Memorie dell' Istituto Geologico dell' Università di Padova, 32*, 1–17.

Bücksteeg, A. (1999). Zur Geologie des Kristallins der Schobergruppe (Osttirol/Österreich). *Aachener Geowissenschaftliche Beiträge, 33*, 1–206.

Budzyń, B., Harlov, D. E., Williams, M. L., & Jercinovic, M. J. (2011). Experimental determination of stability relations between monazite, fluorapatite, allanite, and REE-epidote as a function of pressure, temperature, and fluid composition. *American Mineralogist, 96*, 1547–1567.

Cocherie, A., Legendre, O., Peucat, J., & Koumelan, A. (1998). Geochronology of polygenetic monazites constrained by in situ microprobe Th-U-total lead determination: implications for lead

behavior in monazite. *Geochimica et Cosmochimica Acta, 62*, 2475–2497.

Čopjaková, R., Novák, M., & Franců, E. (2011). Formation of authigenic monazite-(Ce) to monazite-(Nd) from Upper Carboniferous graywackes of the Drahany Upland: roles of the chemical composition of host rock and burial temperature. *Lithos, 127*, 373–385.

Del Rio, P., Barbero, P., Mata, P., & Fanning, C. M. (2009). Timing of diagenesis and very low-grade metamorphism in the eastern sector of the Sierra de Cameros (Iberian Range, Spain): a U-Pb SHRIMP study on monazite. *Terra Nova, 21*, 438–445.

DeWolf, C. P., Belshaw, N. S., & O′Nions, R. K. (1993). A metamorphic history from micron-scale $^{207}Pb/^{206}Pb$ chronometry of Archean monazite. *Earth and Planetary Science Letters, 120*, 207–220.

Evans, J. A., Jalasiewicz, J. A., Fletcher, I. R., Rasmussen, B., & Pearce, N. J. G. (2002). Dating diagenetic monazite in mudrocks: constraining the oil window? *Special Publication of the Geological Society, 159*, 619–622.

Exner, Ch. (1962). Die Perm-Trias-Mulde des Gödnachgrabens an der Störungslinie von Zwischenbergen (Kreuzeckgruppe, östlich Lienz). *Verhandlungen der Geologischen Bundesanstalt, 1962*, 24–27.

Faryad, S. W., & Chakraborty, S. (2005). Duration of Eo-Alpine metamorphic events obtained from multicomponent diffusion modeling of garnet: a case study from the Eastern Alps. *Contributions to Mineralogy and Petrology, 150*, 306–318.

Frey, M., Desmons, J., Neubauer, F. (1999). Metamorphic maps of the Alps. *Published by the editors and as enclosure to the Schweizerische Mineralalogische und Petrographische Mitteilungen, 79/1*.

Frey, M., Desmons, J., & Neubauer, F. (1999b). The new metamorphic map of the Alps: introduction. *Schweizerische Mineralalogische und Petrographische Mitteilungen, 79*, 1–4.

Gaidies, F., Abart, R., de Capitani, C., Schuster, R., Connolly, J. A. D., & Reusser, E. (2006). Characterization of polymetamorphism in the Austroalpine basement east of the Tauern Window using garnet isopleth thermobarometry. *Journal of Metamorphic Geology, 24*, 451–475.

Gaidies, F., Krenn, E., de Capitani, C., & Abart, R. (2008). Coupling forward modelling of garnet growth with monazite geochronology: an application to the Rappold Complex (Austroalpine crystalline basement). *Journal of Metamorphic Petrology, 26*, 775–793.

Ganguly, J., Cheng, W., & Tirone, M. (1996). Thermodynamics of aluminosilicate garnet solid solution: new experimental data, an optimized model, and thermometric applications. *Contributions to Mineralogy and Petrology, 123*, 137–151.

Gratz, R., & Heinrich, W. (1997). Monazite-xenotime thermobarometry: experimental calibration of the miscibility gap in the binary system CePO4 -YPO4. *American Mineralogist, 82*, 772–780.

Habler, G., & Thöni, M. (2001). Preservation of Permo-Triassic low-pressure assemblages in the Cretaceous high-pressure metamorphic Saualpe crystalline basement (Eastern Alps, Austria). *Journal of Metamorphic Geology, 19*, 679–697.

Heinrich, W., Andrehs, G., & Franz, G. (1997). Monazite-xenotime miscibility gap thermometry. I. An empirical calibration. *Journal of Metamorphic Geology, 15*, 3–16.

Hoinkes, G., Koller, F., Rantitsch, G., Dachs, E., Höck, V., Neubauer, F., et al. (1999). Alpine metamorphism of the Eastern Alps. *Schweizerische Mineralalogische und Petrographische Mitteilungen, 79*, 155–181.

Hoke, L. (1990). The Altkristallin of the Kreuzeck Mountains, SE Tauern Window, Eastern Alps - basement crust in a convergent plate boundary zone. *Jahrbuch der Geologischen Bundesanstalt, 133*, 5–87.

Holland, T. J. B., & Powell, R. (1990). An enlarged and updated internally consistent thermodynamic dataset with uncertainties and correlations: the system K2O-Na2O-CaO-MgO-MnO-FeO-Fe2O3-Al2O3-TiO2-SiO2-C-H2-O2. *Journal of Metamorphic Geology, 8*, 89–124.

Holland, T. J. B., & Powell, R. (1998). An internally consistent thermodynamic data set for phases of petrological interest. *Journal of Metamorphic Geology, 16*, 309–343.

Janots, E., Brunet, F., Goffé, B., Poinssot, C., Burchard, M., & Cemič, L. (2007). Thermochemistry of monazite-(La) and dissakisite (La): implications for monazite and allanite stability in metapelites. *Contributions to Mineralogy and Petrology, 154*, 1–14.

Janots, E., Engi, M., Berger, A., Allaz, J., Schwarz, J.-O., & Spandler, C. (2008). Prograde metamorphic sequence of REE minerals in pelitic rocks of the Central Alps: implications for allanite–monazite–xenotime phase relations from 250 to 610 °C. *Journal of Metamorphic Geology, 26*, 509–526.

Janots, E., Negro, F., Brunet, F., Goffé, B., Engi, M., & Bouybaouene, M. L. (2006). Evolution of the REE mineralogy in HP-LT metapelites of the Sebtide complex, Rif, Marocco: monazite stability and geochronology. *Lithos, 87*, 214–234.

Kingsbury, J. A., Miller, C. F., Wooden, J. L., & Harrison, T. M. (1993). Monazite paragenesis and U-Pb systematics in rocks of the eastern Mojave Desert, California, U.S.A., implications for thermochronometry. *Chemical Geology, 110*, 147–167.

Krenn, E., & Finger, F. (2004). Metamorphic formation of Sr-apatite and Sr-bearing monazite in a high pressure rock from the Bohemian Massif. *American Mineralogist, 89*, 1323–1329.

Krenn, E., & Finger, F. (2007). Formation of monazite and rhabdophane at the expense of allanite during Alpine low temperature retrogression of metapelitic basement rocks from Crete, Greece: microprobe data and geochronological implications. *Lithos, 95*, 130–147.

Krenn, E., Janák, M., Fritz, F., Broska, I., & Konečný, P. (2009). Two types of metamorphic monazite with contrasting La/Nd, Th and Y signature in a (ultra) high pressure metapelite from the Pohorje Mountains, Slovenia: indications for a pressure-depended REE exchange between apatite and monazite? *American Mineralogist, 94*, 801–815.

Krenn, E., Ustaszewski, K., & Finger, F. (2008). Detrital and newly formed metamorphic monazite in amphibolite-facies metapelites from the Motajica Massif, Bosnia. *Chemical Geology, 254*, 164–174.

Kryza, R., Zalasiewicz, J. A., Charnley, N., Milodowski, A. E., Kostylew, J., & Tyszka, R. (2004). In situ growth of monazite in anchizonal to epizonal mudrocks: first record from the Variscan accretionary prism of the Kaczawa Mountains, West Sudetes, SW Poland. *Geologia Sudetica, 36*, 39–51.

Lanzirotti, A., & Hanson, G. N. (1996). Geochronology and geochemistry of multiple generations of monazite from Wepawaug Schist, Connecticut, USA: implications for monazite stability in metamorphic rocks. *Contributions to Mineralogy and Petrology, 125*, 332–340.

Linner, M., Thöni, M., & Richter, W. (2000). Exhumation history of Eo-Alpine high-pressure rocks in the Austroalpine Schober basement, Eastern Alps. *Terra Nostra, 1*, 69.

Ludwig, K. (2001). Users Manual for Isoplot/Ex (rev. 2.49): A Geochronological Toolkit for Microsoft Excel. (p. 55) Berkeley Geochronology Center, Special Publication, 1a.

Martins, L., Vlach, S. R. F., & Janasi, V. D. (2009). Reaction microtextures of monazite: correlation between chemical and age domains in the Nazare Paulista migmatite, SE Brazil. *Chemical Geology, 261*, 271–285.

Montel, J.-M., Foret, S., Veschambre, M., Nicollet, C., & Provost, A. (1996). Electron microprobe dating of monazite. *Chemical Geology, 131*, 37–51.

Neubauer, F., Hoinkes, G., Sassi, F. P., Handler, R., Höck, V., Koller, F., et al. (1999). Pre-Alpine metamorphism in the Eastern Alps. *Schweizerische Mineralalogische und Petrographische Mitteilungen, 79*, 41–62.

Oxburgh, E.R., Lambert, R.S., Baadsgard, H., Simons, J.G. (1966). Potassium-Argon age studies across the southeast margin of the Tauern window in the Eastern Alps. *Verhandlungen der Geologischen Bundesanstalt,* 17–33.

Petrík, I., & Konečný, P. (2009). Metasomatic replacement of inherited metamorphic monazite in a biotite-garnet granite from the Nízke Tatry Mountains, Western Carpathians, Slovakia: chemical dating and evidence for disequilibrium melting. *American Mineralogist, 94*, 957–974.

Poitrasson, F., Chenery, S., & Bland, D. J. (1996). Contrasted monazite hydrothermal alteration mechanisms and their geochemical implications. *Earth and Planetary Science Letters, 145*, 79–96.

Poitrasson, F., Chenery, S., & Shepherd, T. J. (2000). Electron microprobe and LA-ICP-MS study of monazite hydrothermal alteration: implications for U-Th–Pb geochronology and nuclear ceramics. *Geochimica et Cosmochimica Acta, 64*, 3283–3297.

Powell, R., & Holland, T. J. B. (1993). On the formulation of simple mixing models for complex phases. *American Mineralogist, 78*, 1174–1180.

Putnis, A. (2002). Mineral replacement reactions: from macroscopic observations to microscopic mechanisms. *Mineralogical Magazine, 66*, 689–708.

Putnis, A. (2009). Mineral replacement reactions. In: K.D. Putirka, F.J. Tepley (Eds.), *Minerals, inclusions and volcanic processes. Reviews in Mineralogy and Geochemistry*, 70 (pp. 87–124).

Pyle, J. M. (2006). Temperature-time paths from phosphate accessory phase paragenesis in the Honey Brook Upland and associated cover sequence, SE Pennsylvania, USA. *Lithos, 88*, 201–232.

Pyle, J. M., & Spear, F. S. (1999). Yttrium zoning in garnet: coupling of major and accessory phases during metamorphic reactions. *Geological Materials Research, 1*, 1–49.

Pyle, J. M., & Spear, F. S. (2003). Four generations of accessory-phase growth in low-pressure migmatites from SW New Hampshire. *American Mineralogist, 88*, 338–351.

Pyle, J. M., Spear, F. S., Rudnick, R., & Mcdonough, W. (2001). Monazite-xenotime-garnet equilibrium in metapelites and a new monazite-garnet thermometer. *Journal of Petrology, 42*, 2083–2107.

Rasmussen, B., Fletcher, I. R., & McNaughton, N. J. (2001). Dating low grade metamorphic events by SHRIMP U-Pb analysis of monazite in shales. *Geol, 29*, 963–966.

Rasmussen, B., & Muhling, J. R. (2007). Monazite begets: evidence for dissolution of detrital monazite and reprecipitation of syntectonic monazite during low-grade regional metamorphism. *Contributions to Mineralogy and Petrology, 154*, 675–689.

Rasmussen, B., & Muhling, J. R. (2009). Reactions destroying detrital monazite in greenschist-facies sandstones from the Witwatersrand basin, South Africa. *Chemical Geology, 264*, 311–327.

Read, D., Cooper, D. C., & McArthur, J. M. (1987). The composition and distribution of nodular monazite in the Lower Palaeozoic rocks of Great Britain. *Mineralogical Magazine, 51*, 271–280.

Rubatto, D., Hermann, J., & Buick, I. S. (2006). Temperature and bulk composition control on the growth of monazite and zircon during low-pressure anatexis (Mount Stafford, central Australia). *Journal of Petrology, 47*, 1973–1996.

Schmid, S. M., Fügenschuh, B., Kissling, E., & Schuster, R. (2004). Tectonic map and overall architecture of the Alpine orogen. *Eclogae Geologicae Helvetiae, 97*, 93–117.

Schulz, B. (1990). Prograde-retrograde P-T-t-de-formation path of Austroalpine micaschists du-ring Variscan continental collision (Eastern Alps). *Journal of Metamorphic Geology, 8*, 629–643.

Schulz, B. (1993a). Mineral chemistry, geother-mo-barometry and pre-Alpine high-pressure meta-morphism of eclogitic amphibolites and mica schists from the Schobergruppe, Austroalpine basement, Eastern Alps. *Mineralogical Magazi-ne, 57*, 189–202.

Schulz, B. (1993b). P-T-deformation paths of Variscan metamorphism in the Austroalpine basement: controls on geothermobarometry from microstructures in progressively deformed metapelites. *Schweizerische Mineralogische und Petrographische Mitteilungen, 73*, 257–274.

Schulz, B., Finger, F., Krenn, E. (2005). Auflösung variskischer, permischer und alpidischer Ereignisse im polymetamorphen ostalpinen Kristallin südlich der Tauern mit EMS-Datierung von Monazit. *Arbeitstagung der Geologischen Bundesanstalt Österreich, 141–153*.

Schulz, B., Steenken, A., Siegesmund, S. (2008). Geodynamics of an Alpine terrane—the Austroalpine basement to the south of the Tauern Window as a part of the Adriatic Plate. In: S. Siegesmund, B. Fügenschuh., & N. Froitzheim (Eds.), Tectonic aspects of the Alpine-Dinaride-Carpathian system, 298, (pp. 5–43). Geological Society of london special publications.

Schulz, B., & von Raumer, J. F. (2011). Detection of a pre-Variscan metamorphic event by EMP monazite dating and thermobarometry of garnet metapelites in the Alpine External Aiguilles Rouges Massif. *Swiss Journal of Geosciences, 104*, 67–79.

Schuster, R., Koller, F., Höck, V., Hoinkes, G., & Bousquet, R. (2004). Explanatory notes to the map: metamorphic structure of the Alps—Metamorphic evolution of the Eastern Alps. *Mitteilungen der Österreichischen Mineralogischen Gesellschaft, 149*, 175–199.

Schuster, R., Scharbert, S., Abart, R., & Frank, W. (2001). Permo-Triassic extension and related HT/LP metamorphism in the Austroalpine—Southalpine realm. *Mitteilungen der Gesellschaft der Geologie und Bergbaustudenten Österreichs, 45*, 111–141.

Schuster, R., & Stüwe, K. (2008). Permian metamorphic events in the Alps. *Geol, 36*, 603–606.

Schuster, R., & Thöni, M. (1996). Permian garnet: indications for a regional Permian metamorphism in the southern part of the Austroalpine basement units. *Mitteilungen der Österreichischen Geologischen Gesellschaft, 141*, 219–221.

Seydoux-Guillaume, A.-M., Wirth, R., Heinrich, W., & Montel, J. M. (2002). Experimental determination of Thorium partitioning between monazite and xenotime using analytical electron microscopy and X-ray diffraction Rietveld analysis. *European Journal of Mineralogy, 14*, 869–878.

Spear, F. S. (2010). Monazite–allanite phase relations in metapelites. *Chemical Geology, 279*, 55–62.

Spear, F. S., Cheney, J. T., Pyle, J. M., Harrison, T. M., & Layne, G. (2008). Monazite geochronology in central New England: evidence for a fundamental terrain boundary. *Journal of Metamorphic Geology, 26*, 317–329.

Steidl, M., Tropper, P., Linner, M., & Schuster, R. (2009). Petrology of metapelites from the Michelbach Complex (Defreggen Complex, Eastern Tyrol). *Mitteilungen der Österreichischen Geologischen Gesellschaft, 155*, 149.

Steidl, M., Tropper, P., Linner, M., & Schuster, R. (2010a). Unravelling the polymetamorphic (Variscan vs. Permian) history of the Michlbach Complex (Deffregger Alps, East Tyrol) by using REE phosphates (monazite, xenotime). *Journal of Alpine Geology, 52*, 234–235.

Steidl, M., Tropper, P., Linner, M., & Schuster, R. (2010b). Petrology of the polymetamorphic metapelites from the Michlbach Complex (Defreggen Complex, East Tyrol). *Journal of Alpine Geology, 52*, 235.

Suzuki, K., Adachi, M., & Tanaka, T. (1991). Middle Precambrian provenance of Jurassic sandstone in the Mino Terrane, central Japan: th-U-total Pb evidence from an electron microprobe monazite study. *Sedimentary Geology, 75*, 141–147.

Thöni, M., & Miller, Ch. (1996). Garnet Sm-Nd data from the Saualpe and the Koralpe (Eastern Alps, Austria): chronological and P-T constraints on the thermal and tectonic history. *Journal of Metamorphic Geology, 14*, 453–466.

Todd, C. S. (1998). Limits on the precision of geobarometry at low grossular and anorthite content. *American Mineralogist, 83*, 1161–1167.

Troll, G., Baumgartner, S., & Daiminger, W. (1980). Zur Geologie der südwestlichen Schobergruppe (Osttirol, Österreich). *Mitteilungen der Gesellschaft der Geologie- und Bergbaustudenten Österreichs, 26*, 277–295.

Troll, G., Forst, R., Söllner, F., Brack, W., Kohler, H., & Müller-Sohnius, D. (1976). Über Bau, Alter und Metamorphose des Altkristallins der Schobergruppe, Osttirol. *Geologische Rundschau, 65*, 483–511.

Troll, G., & Hölzl, E. (1974). Zum Gesteinsaufbau des Altkristallins der zentralen Schobergruppe, Osttirol. *Jahrbuch der Geologischen Bundesanstalt, 117*, 1–16.

Wan, Y. S., Song, T. R., Liu, D. Y., Yang, T. N., Yin, X. Y., Chen, Z. Y., et al. (2007). Mesozoic monazite in Neoproterozoic metasediments: evidence for low-grade metamorphism of Sinian Sediments during Triassic Continental Collision, Liaodong Peninsula, NE China. *Geochemical Journal, 41*, 47–55.

Wilby, P. R., Page, A. A., Zalasiewicz, J. A., Milodowski, A. E., Williams, M., & Evans, J. A. (2007). Syntectonic monazite in low-grade mudrocks: a potential geochronometer for cleavage formation? *Journal of the Geological Society, 164*, 53–56.

Wing, B., Ferry, J., & Harrison, T. (2003). Prograde destruction and formation of monazite and allanite during contact and regional metamorphism of pelites: petrology and geochronology. *Contributions to Mineralogy and Petrology, 145*, 228–250.

Zhu, X. K., & O'Nions, R. K. (1999a). Zonation of monazite in metamorphic rocks and its implications for high temperature thermochronology: a case study from the Lewisian Terrain. *Earth and Planetary Science Letters, 171*, 209–220.

Zhu, X. K., & O'Nions, R. K. (1999b). Monazite chemical composition: some implications for monazite geochronology. *Contributions to Mineralogy and Petrology, 137*, 351–363.